analytical chemistry

pubs.acs.org/ac Article

Top-Down Approach to Retention Time Prediction in Comprehensive Two-Dimensional Gas Chromatography−Mass Spectrometry

Meriem Gaida,* Flavio A. Franchina, Pierre-Hugues Stefanuto, and Jean-François Focant

Cite This: *Anal. Chem.* 2022, 94, 17081−17089 Read Online

ACCESS | Metrics & More | Article Recommendations | Supporting Information

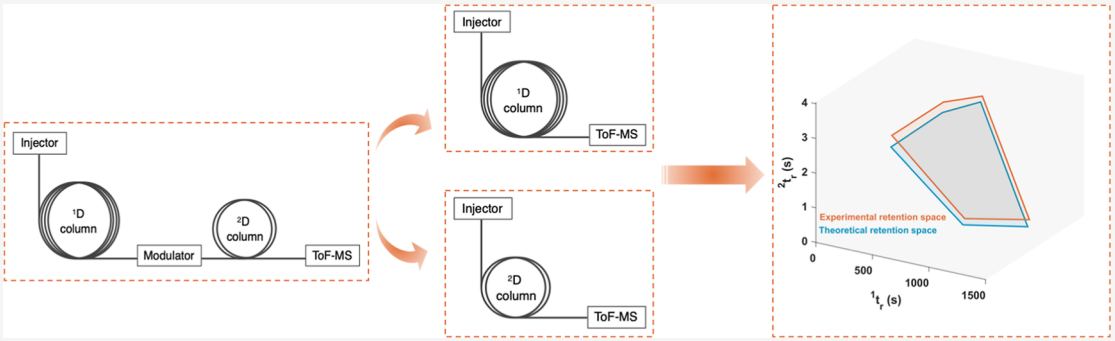

ABSTRACT: In this contribution, we describe a novel modeling approach to predicting retention times (t_r) in comprehensive two-dimensional gas chromatography coupled to time-of-flight mass spectrometry (GC × GC−ToF-MS) with a particular emphasis on the second-dimension (^{2}D) retention time predictions (^2t_r). This approach is referred to as a "top-down" approach in that it breaks down the complete GC × GC separation into two independent one-dimensional gas chromatography separations (1D-GC). In this regard, both dimensions, that is, first dimension (^{1}D) and second dimension (^{2}D) are treated separately, and the cryogenic modulator is simply considered as a second consecutive injection device. Separate 1D-GC t_r predictions are performed on both dimensions using the same flow rate as the one deployed in the conventional GC × GC system. The separate t_r predictions are then combined to account for the two-dimensional separation. This model was applied to 24 analytes from 2 standard mixtures (Grob Test Mix and Fragrance Materials Test Mix) and assessed across 9 GC × GC chromatographic conditions. The experimental and predicted chromatographic retention space occupations were assessed by using the convex hull approach defined by the Delaunay triangulation. The predicted percentage of space occupation corresponded favorably with the experimental values. Furthermore, the top-down approach enabled an accurate prediction of the ^2t_r of all investigated analytes, providing an average ^2t_r modeling error of 0.26 ± 0.01 s.

Comprehensive two-dimensional gas chromatography (GC × GC) was first introduced in 1991 by Liu and Phillips[1] and has come a long way since. It is now considered a cornerstone technique in the analysis of complex samples derived from considerably different fields, such as metabolomics,[2] forensics,[3] and food.[4] Its unprecedented capacity to provide trace-level identification and quantification is enabled by its orthogonal separation mechanisms and increased peak capacity and further corroborated by its hyphenation to mass spectrometry (MS), especially through the use of time-of-flight mass spectrometry (ToF-MS), which allows high acquisition rates and MS deconvolution. Furthermore, GC × GC undoubtedly owes its success to the presence of the unique modulation process considered a key factor in the chromatographic separation.[5] The modulator role consists of transferring the first-dimension (^{1}D) column eluate to the second-dimension (^{2}D) column during a specific time period referred to as the modulation period (P_M) while preserving the quality of the separation achieved during the first dimension. The P_M value is carefully chosen to provide an appropriate sampling frequency relative to the ^{1}D peak width to maximize the ^{2}D peak capacity.

Evidently, the addition of a second chromatographic separation dimension has its advantages when handling the wealth of information provided by complex and challenging data sets. However, higher resolution and increased sensitivity carry a price in terms of optimization and data processing.

Received: July 18, 2022
Accepted: November 16, 2022
Published: November 29, 2022

https://doi.org/10.1021/acs.analchem.2c03107
Anal. Chem. 2022, 94, 17081−17089

Significant challenges arise during the optimization process due to the complex interactions between all involved experimental parameters.[6] In this regard, establishing robust modeling approaches can be of great help. On the one hand, they help reduce the time dedicated to the optimization process by guiding, for instance, the selection of optimal column sets[7] and adequate experimental settings.[8] On the other hand, they help shift the analytical chemist's focus to the more onerous, tedious, and time-consuming data-processing step. In this respect, considerable modeling efforts were dedicated to studying the GC × GC separation mechanisms, most of which have patently focused on modeling the thermodynamics of the separation.[9−18]

Typically, thermodynamic-based modeling relates the chromatographic retention data to relevant thermodynamic indices, namely, enthalpy (ΔH), entropy (ΔS), and molar heat capacity (ΔC_p), and enables a better description of the solute-stationary phase interactions.[19] In fact, in gas chromatography, ΔH is viewed as a measurement of the dissolution energy difference of an analyte between the stationary and mobile phases. Moreover, ΔS measurements help to assess the analytes' change of degrees of freedom when they travel between the stationary and mobile phases.[20] In thermodynamic modeling, the GC × GC separation is perceived as a kinetic process during which the analytes' migration through the column is governed by the kinetics of exchange of the analytes between the mobile and stationary phases.[21] In this regard, the analytes' retention times (t_r) are predicted by tracking their movements through the column using the time summation model.[22] Thermodynamic modeling has been widely discussed in the literature and multiple models were proposed to provide better characterization of the intermolecular interactions between the analytes and the stationary phase.[9,14,19,23]

A GC × GC separation is also perceived as a dynamic process involving parameters that experience changes both in time and in space, that is, temperature, carrier gas viscosity and velocity, and pressure. In fact, during the chromatographic separation, the analytes pass through multiple thermal zones (^{1}D oven, modulator, ^{2}D oven, and transfer line), all of which are regulated by specific temperature programs. Through this transition, fast temperature changes occur and affect both the carrier gas viscosity and velocity. These perpetual variations make the modeling of the chromatographic separation process quite intricate.

In most of the previously reported studies, minimal modeling errors were reported for the first-dimension retention times (^1t_r). However, reaching the same modeling precision for the second-dimension retention times (^2t_r) continues to be a significant challenge, especially for systems using cryogenic modulation due to insufficient assessment of the impact of the analytes' sorption and desorption on their retention behavior in the modulator. For instance, maximum ^2t_r deviations of 1.2 and 0.4 s along with a ^2t_r relative deviation of 7% were reported in the literature for cryogenically modulated systems.[9,11,13] Contrastingly, average ^2t_r relative errors (REs) of 2.22 and 2.09% were reported for flow-modulated systems.[10,18] The lack of direct user pressure control in cryogenically modulated systems, except for the pressure control at the inlet, was argued to be one of the main contributors to this difference.[15] Multiple efforts were dedicated to decreasing the ^{2}D retention time modeling errors. For instance, Jaramillo *et al.*[15] highlighted the dependence of the modeling errors on the carrier gas velocity and the analytes elution temperatures and established a correction model in that respect. The model enabled a decrease in the average ^2t_r modeling error from 0.197 to 0.017 s. By acknowledging the effect of temperature and pressure on the equilibrium constant, Burel *et al.*[14] introduced an alternative prediction model that contrasted with the classical description of the equilibrium constant and managed to decrease the second-dimension modeling error from 7.3 to 2.2%.

Most of the reported modeling works have focused on modeling the GC × GC separation under atmospheric outlet conditions through the use of a flame ionization detector in an attempt to ease the calculation process.[9,10,12,14,15,18,24] However, in light of the increasing complexity of the studied samples, GC × GC is usually operated with a high-resolutionToF-MS ((HR)ToF-MS) for better sample characterization and identification. For instance, GC × GC−(HR)ToF-MS has nowadays become a method of choice in the characterization of volatile organic compounds issued from biological samples and has proven its unique capacity to identify potential biomarkers that can be used for the future development of novel medical diagnostic tools.[2,25,26] Therefore, it can be of high relevance to develop modeling approaches that can accurately describe the analyte's retention behavior in a GC × GC−MS setting and hence help in the optimization of the separation of complex biological samples.

So far, the majority of the theoretical work conducted in GC × GC solely focuses on modeling the integrity of the two-dimensional separation. Nevertheless, in this work, we propose an alternative modeling approach that breaks down the GC × GC system into two separate individual one-dimensional GC (1D-GC) subsystems. In this scheme, 1D-GC retention time predictions will be performed on separate ^{1}D and ^{2}D columns and then combined to describe the two-dimensional separation space. The predictions of the ^{1}D retention times are described in a previous publication.[27] Thus, in this work, we will mainly focus on predicting the ^{2}D retention times of 24 analytes under vacuum outlet conditions. The prediction accuracy will be evaluated using a total of nine different GC × GC operating conditions.

PRINCIPLES AND THEORY

In this study, the GC × GC separation is broken down into two individual 1D-GC separations, and each dimension, ^{1}D and ^{2}D, is modeled separately, and the cryogenic modulator is simply considered as a consecutive second injection device. Both dimensions are modeled at the same flow rate (F) as the one used in the conventional GC × GC separation. The modeling of the first-dimension retention times is discussed in a previous publication.[27] Hence, the present work will be centered on modeling the second-dimension retention times. Typically, it is believed that the ^{2}D separation in GC × GC is so fast that it occurs isothermally.[24] Thus, the ^2t_r of the investigated compounds can be modeled isothermally at each analyte's first-dimension elution temperature ($^1T_{el}$) with the acknowledgment of the ^{2}D oven temperature offset. This final temperature ($^1T_{el}$ + ^{2}D oven offset) will be referred to as the ^{2}D elution temperature ($^2T_{el}$).

This study aims at mirroring, to a certain extent, the conventional GC × GC separation by reducing it to two 1D-GC settings. In this regard, the same flow rate (F = 1.2 mL min^{-1}) as the one used in the conventional GC × GC run is applied to all 1D-GC separations carried out on the ^{2}D

https://doi.org/10.1021/acs.analchem.2c03107
Anal. Chem. 2022, 94, 17081−17089

column. However, such a framework entails a negative column inlet pressure (P_{in}). As a matter of fact, performing isothermal 1D-GC separations on the noticeably shorter ^{2}D column requires relatively high flow rates. For instance, an isothermal separation performed at 70 °C on a 2 m GC column requires a minimum F of 6 mL min^{-1}. Hence, we sought to put in place an adequate experimental setup that would enable us to push the separation conditions to the limits of the hardware. Hereof, a deactivated capillary (DC), with a specific calculated length (L = 8.50 m), is added before the ^{2}D column to ensure a positive column head pressure. Due to the presence of various thermal zones (^{1}D oven, ^{2}D oven, and transfer line), a second shorter DC (L = 0.53 m) is added after the ^{2}D column to ensure that the ^{2}D separation occurs at the main oven temperature setting and to ease the calculation process by isolating the GC column from the MS detector. All capillaries are of the same diameter. The experimental design is described in Figure 1.

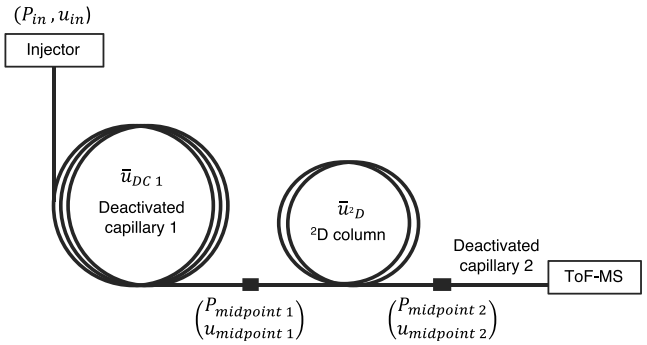

Figure 1. Schematic of the 1D-GC experimental design used to mimic the second-dimension (^{2}D) comprehensive GC (GC × GC) separation. The addition of the first and second DCs (DC 1 and DC 2) enables the discrete modeling of the ^{2}D retention times (^2t_r).

The discrete modeling of the ^{2}D column separation is achieved through a series of calculations. Due to the presence of a mass spectrometer detector, the current system operates under a strong gas decompression and a single pressure control point. Using the concept of a vacuum extension of a tube introduced and described by Blumberg,[28] we consider all connected capillaries as one tube with its outlet being at vacuum, and the u_{in}, $P_{midpoint1}$, $P_{midpoint2}$, $u_{midpoint1}$, and $u_{midpoint2}$ values can be calculated (Figure 1).

The carrier gas velocity at the inlet of the first DC (u_{in}) is given by

$$u_{in} = \frac{P_{in}}{2\Omega} \tag{1}$$

where Ω is termed as the vacuum-extended pneumatic resistance,[28] defined by

$$\Omega = L\eta_T \frac{32}{i_d^2} \tag{2}$$

L is the length of the experimental design, i_d is the diameter of the capillaries, and η_T is the carrier gas (helium) viscosity (eq 3).

$$\eta_T = 18.63\left(\frac{T}{273}\right)^{0.6958-0.0071\left(\frac{T-273}{273}\right)} \tag{3}$$

Under vacuum outlet conditions,[29] the dead time (t_m) is calculated using eq 4. Rearrangements of this equation enable the calculation of the inlet pressure (P_{in}).

$$t_m = \frac{128L^2}{3i_d^2}\frac{\eta_T}{P_{in}} \tag{4}$$

The pressure (P_x) and the velocity (u_x) at an arbitrary location x in the experimental design (Figure 1) are calculated using eqs 5 and 6. Both equations enable the calculation of the pressures and velocities at the junction between the first DC and the GC column ($P_{midpoint1}$, $u_{midpoint1}$) and at the interconnection point of the GC column and the second DC ($P_{midpoint2}$, $u_{midpoint2}$).

$$P_x = P_{in}\sqrt{1 - \frac{x}{L}} \text{ with } 0 \le x \le L \tag{5}$$

$$u_x = \frac{u_{in}}{\sqrt{1 - \frac{x}{L}}} \text{ with } 0 \le x \le L \tag{6}$$

The average carrier gas velocities in the first DC ($\bar{u}_{DC\,1}$) and in the ^{2}D column ($\bar{u}_{^2D}$) are calculated using one form of the Poiseuille equation (eq 7). In the present study, P_{out} corresponds to either $P_{midpoint1}$ or $P_{midpoint2}$.

$$\bar{u} = \frac{(P_{in} - P_{out})\left(\frac{P_{in}}{P_{out}} + 1\right)i_d^2}{64L\eta_T} \tag{7}$$

The retention times in the ^{2}D column are calculated based on eq 8.

$$^2t_r = \frac{(1 + k_T)L_{^2D\ column}}{\bar{u}_{^2D}} \tag{8}$$

The isothermal retention factors (k_T), for each studied analyte, on the ^{2}D column are calculated using a three-parameter model that involves a thermodynamic treatment of the GC equilibrium constant (K_T)[23] (eq 9). A, B, and C are constant terms related to thermodynamic indices, namely, enthalpy (ΔH), entropy (ΔS), and molar heat capacity (ΔC_p).[19]

$$\ln(K_T) = A + B\frac{1}{T} + C\ \ln(T) \tag{9}$$

$$k_T = \frac{K_T}{\beta} \tag{10}$$

β is the phase ratio defined by eq 11, in which d_f corresponds to the stationary phase film thickness.

$$\beta = \frac{i_d}{4d_f} \tag{11}$$

EXPERIMENTAL SECTION

Test Standards. For this study, the Grob Test Mix and the Fragrance Materials Test Mix (Restek, Bellefonte, PA, USA) were used. They each included 12 compounds covering a broad range of chemical families (Table 1). Thus, accurate predictions of their retention times would provide a reliable indication of the model's performance. Using such commercially available standard mixtures allows future potential

https://doi.org/10.1021/acs.analchem.2c03107
Anal. Chem. 2022, 94, 17081−17089

Table 1. Measured and Predicted Second-Dimension Retention Times (^2t_r) for the 24 Studied Compounds

no	compound[a]	meas.[b] ^2t_r (s)	pred. ^2t_r (s)	error (s)
1	2,3-butanediol	2.66	2.42	0.24
2	decane	1.93	1.69	0.24
3	1-octanol	2.60	2.32	0.28
4	undecane	1.97	1.73	0.25
5	nonanal	2.72	2.43	0.30
6	2,6-dimethylphenol	3.66	3.34	0.33
7	2-ethylhexanoic acid	2.52	2.23	0.30
8	2,6-xylidine	4.16[c]	3.83	0.33
9	C-10 FAME	2.61	2.34	0.27
10	dicyclohexylamine	2.98	2.71	0.27
11	C-11 FAME	2.61	2.35	0.25
12	C-12 FAME	2.62	2.36	0.26
13	ethyl butyrate	2.33	1.99	0.34
14	D-limonene	2.53	2.23	0.29
15	eucalyptol	2.71	2.43	0.28
16	benzoic acid	3.62	3.31	0.30
17	geraniol	2.98	2.73	0.25
18	cinnamic aldehyde	0.60	0.41	0.19
19	hydroxycitronellal	3.32	3.09	0.22
20	thymol	3.43	3.19	0.24
21	cinnamyl alcohol	0.39	0.20	0.19
22	vanillin	1.11	0.92	0.20
23	cinnamyl acetate	4.04[c]	3.86	0.18
24	benzyl salicylate	0.77	0.55	0.21

[a]Compounds 1−12 are part of the Grob Test Mix, whereas compounds 13−24 belong to the Fragrance Materials Test Mix. Both samples were injected separately. [b]All measurements were performed using a ramp rate of 7 °C min^{-1} and a modulation period equal to 4 s. [c]Wrapped-around compounds. For the sake of comparison, one modulation period was added to their second-dimension retention times (^2t_r).

replications and benchmarking to other approaches by other groups.

GC × GC−ToF-MS Analyses. All separations were carried out on a Pegasus BT 4D GC × GC−ToF-MS instrument equipped with a cryogenic modulator (LECO Corp., St Joseph, MI, USA). The GC × GC column set consisted of a ^{1}D nonpolar crossbond diphenyl dimethyl polysiloxane column (Rxi-5ms, Restek, Bellefonte, PA, USA) with a nominal geometry of 30 m × 0.25 mm i_d × 0.25 μm d_f and a ^{2}D midpolarity crossbond phase column (Rxi-17Sil MS, Restek, Bellefonte, PA, USA) with a nominal geometry of 2 m × 0.25 mm i_d × 0.25 μm d_f. The actual column lengths were measured with exactitude: L (^{1}D column) = 30.37 m and L (^{2}D column) = 1.94 m. A helium flow rate of 1.2 mL min^{-1} was used for all separations (1D-GC and GC × GC). Three temperature ramps (3, 5, and 7 °C min^{-1}) along with three modulation periods (P_M = 3, 4, and 5 s) were evaluated in this study. For Grob Test Mix separations, the GC oven was set to an initial temperature of 45 °C (held for 2 min) and then ramped to a final temperature of 200 °C (held for 5 min). For Fragrance Materials Test Mix separations, the temperature program was initialized at 50 °C (held for 2 min) and then increased to a final temperature of 270 °C (held for 5 min). The ^{2}D oven and the modulator were, respectively, controlled by +5 and +20 °C offsets relative to the main GC oven. The MS transfer line was set at 250 °C and the split/splitless injector at 300 °C. All injections were performed in triplicates.

GC−ToF-MS Analyses. For the calculation of the A, B, and C parameters of all studied analytes (eq 9), isothermal retention data, that is, retention times and dead times, were collected on the midpolarity crossbond phase column (Rxi-17Sil MS) with a nominal geometry of 15 m × 0.25 mm i_d × 0.25 μm d_f. Isothermal temperature programs ranging from 50 to 170 °C, with 10 °C increments, were used for the data collection. The dead time profile (t_m*vs.* T) of the experimental setup described in Figure 1 was measured isothermally using temperatures varying between 70 and 150 °C, with 5 °C increments. Nitrogen was used as a dead time marker.

Software. All data were processed *via* LECO ChromaTOF software (ver. 5.51.06). Data fittings and retention time predictions were performed using in-house MATLAB (ver. R2019b, MathWorks, MA, USA) codes.

RESULTS AND DISCUSSION

Spatial Profiles of Pressure and Carrier Gas Velocity. For this work, the discrete modeling of the ^{2}D separation hinges on one major assumption. The in-series-coupled capillaries (Figure 1) are considered to form one individual tube subjected to a vacuum outlet due to the presence of a mass spectrometer detector. In this scheme, the retention of the analytes in the GC column can be described through a series of calculations (eqs 5−7). Furthermore, the spatial profiles of pressure and velocity across all involved capillaries can likewise be described. Both parameters are subject to distinct spatial variations and exhibit antagonistic fluctuations in relation to one another. This is particularly true when the system is operated under strong gas decompression conditions. In fact, a significant pressure drop causes a large increase in the carrier gas velocity to ensure that the pressure−velocity product remains constant throughout the entire system. This is demonstrated in the present work frame (Figure 2). Figure 2 displays the velocity and pressure variations solely across the first DC and the GC column at specific distances calculated starting from the inlet. The carrier gas velocity gradually increases across the first DC and then rapidly accelerates near

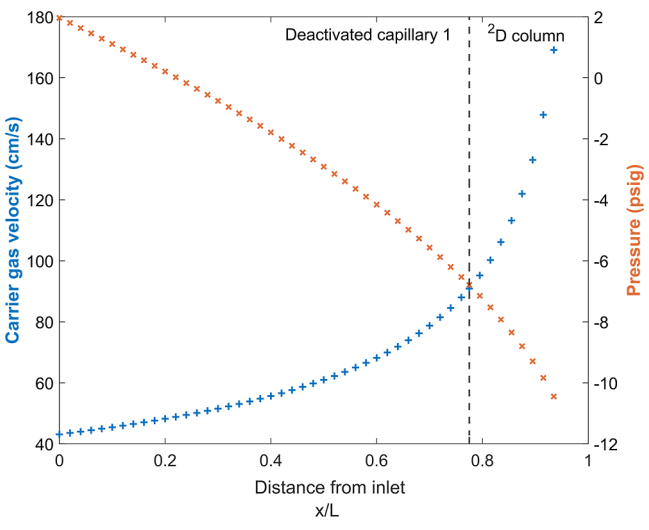

Figure 2. Spatial profiles of pressure and carrier gas velocity along the first DC (DC 1) and the ^{2}D column calculated at the isothermal second-dimension elution temperature ($^2T_{el}$) of 2,6-dimethylphenol. x represents a specific position in the DC 1 or the ^{2}D column with respect to the length of the entire setup (L).

https://doi.org/10.1021/acs.analchem.2c03107
Anal. Chem. 2022, 94, 17081−17089

Table 2. Summary of the Prediction Errors Related to the Modeling of Multiple Experimental GC × GC Conditions

		modulation period (P_M (s))								
		error (s)[b]								
		7 °C min^{-1}			5 °C min^{-1}			3 °C min^{-1}		
no	compound[a]	3	4	5	3	4	5	3	4	5
1	2,3-butanediol	0.24	0.24	0.24	0.28	0.26	0.26	0.31	0.31	0.31
2	decane	0.24	0.24	0.24	0.28	0.28	0.27	0.34	0.35	0.35
3	1-octanol	0.28	0.28	0.29	0.34	0.35	0.36	0.47	0.47	0.46
4	undecane	0.23	0.25	0.23	0.27	0.28	0.27	0.34	0.35	0.34
5	nonanal	0.29	0.30	0.29	0.37	0.36	0.37	0.50	0.51	0.49
6	2,6-dimethylphenol	0.33	0.33	0.31	0.45	0.42	0.43	0.65	0.67	0.63
7	2-ethylhexanoic acid	0.29	0.30	0.28	0.34	0.35	0.33	0.46	0.46	0.45
8	2,6-xylidine	0.37	0.33	0.32	0.46	0.47	0.47	0.70	0.68	0.68
9	C-10 FAME	0.27	0.27	0.28	0.32	0.33	0.32	0.42	0.43	0.44
10	dicyclohexylamine	0.26	0.27	0.27	0.32	0.30	0.31	0.42	0.42	0.41
11	C-11 FAME	0.27	0.25	0.25	0.32	0.30	0.30	0.41	0.41	0.40
12	C-12 FAME	0.25	0.26	0.24	0.30	0.28	0.30	0.37	0.37	0.38
13	ethyl butyrate	0.30	0.34	0.31	0.35	0.34	0.36	0.41	0.41	0.40
14	D-limonene	0.29	0.29	0.29	0.32	0.34	0.35	0.42	0.43	0.48
15	eucalyptol	0.23	0.28	0.23	0.28	0.26	0.25	0.35	0.36	0.39
16	benzoic acid	0.31	0.30	0.35	0.36	0.38	0.43	0.53	0.57	0.61
17	geraniol	0.25	0.25	0.26	0.30	0.28	0.30	0.39	0.40	0.40
18	cinnamic aldehyde	0.24	0.19	0.21	0.30	0.29	0.24	0.40	0.41	0.43
19	hydroxycitronellal	0.24	0.22	0.25	0.29	0.27	0.29	0.41	0.41	0.41
20	thymol	0.23	0.24	0.25	0.29	0.29	0.27	0.40	0.39	0.37
21	cinnamyl alcohol	0.21	0.19	0.20	0.28	0.28	0.26	0.39	0.35	0.39
22	vanillin	0.20	0.20	0.19	0.22	0.21	0.22	0.31	0.27	0.33
23	cinnamyl acetate	0.19	0.18	0.20	0.23	0.18	0.22	0.23	0.26	0.25
24	benzyl salicylate	0.23	0.21	0.25	0.25	0.27	0.27	0.33	0.36	0.36
	total average error (s)	0.26	0.26	0.26	0.31	0.31	0.31	0.42	0.42	0.42
	standard error (s)	±0.01	±0.01	±0.01	±0.01	±0.01	±0.01	±0.02	±0.02	±0.02

[a]Note that compounds 1−12 are part of the Grob Test Mix, whereas compounds 13−24 belong to the Fragrance Materials Test Mix. Both samples were injected separately. [b]The errors reported in the table result from the differences between the measured and the predicted second-dimension retention time (^2t_r).

the end of the GC column. These profiles are calculated isothermally at the $^2T_{el}$ of 2,6-dimethylphenol. Identical behaviors are observed for all other compounds.

Prediction of ^2t_r and the Chromatographic Separation Space. The ^{2}D retention times were calculated isothermally at each analyte's $^2T_{el}$ (eq 8). As previously discussed, the present approach disregards the modulator role in the separation since the GC × GC run is divided into two individual 1D-GC subsystems. However, to make sure that the predicted retention times do not exceed the experimental modulation period the following strategy is implemented.

if calculated $^2t_r \geq P_M$ then

Reported ^2t_r = calculated $^2t_r - nP_M$ with $n = 0,1,2, \ldots$

else

reported ^2t_r = calculated ^2t_r

The Grob Test Mix and the Fragrance Materials Test Mix analytes were separated under nine different GC × GC methods. The deviation between the experimental and predicted ^2t_r will be reported in terms of absolute errors (in seconds) rather than the commonly used REs. In this particular scheme, where a portion of the system is not accounted for in the modeling process (*i.e.*, the modulator), RE calculations are not pertinent and hence deemed not fit to assess the model's performance. Table S1 in the Supporting Information provides the experimental and predicted data for the three temperature programs discussed in the present article. Regardless of the experimental conditions used (Tables 1 and 2), three different ramp rates (7, 5, and 3 °C min^{-1}), and modulation periods P_M (3, 4, and 5 s), the current model consistently underestimated the ^2t_r value, resulting therefore in shorter retention times (Table 1). This is presumably a result of the omission of the modulator during the modeling process. This assumption will be further discussed in the following sections.

The differences between the predicted and measured ^2t_r ranged from 0.18 to 0.34 s, with an average error of 0.26 s (±0.01 s) across all studied compounds (Table 1). Typically, cryogenically modulated peaks present peak widths ranging between 0.1 and 0.2 s. In this regard, the modeling errors could be estimated to 2−3 peak widths. Additionally, the comparison of multiple commercially available GC × GC software highlighted the presence of an average difference of 0.15 s between the reported ^2t_r when changing software due to differences in the data transformation algorithms.[30] In light of this comparison, the errors yielded by the present approach do not seem outrageous but rather lie in quite a reasonable range.

No specific trends were noticed within a particular temperature program as the modeling errors were dispersed in a random fashion (Figure 3). However, the modeling errors

https://doi.org/10.1021/acs.analchem.2c03107
Anal. Chem. 2022, 94, 17081−17089

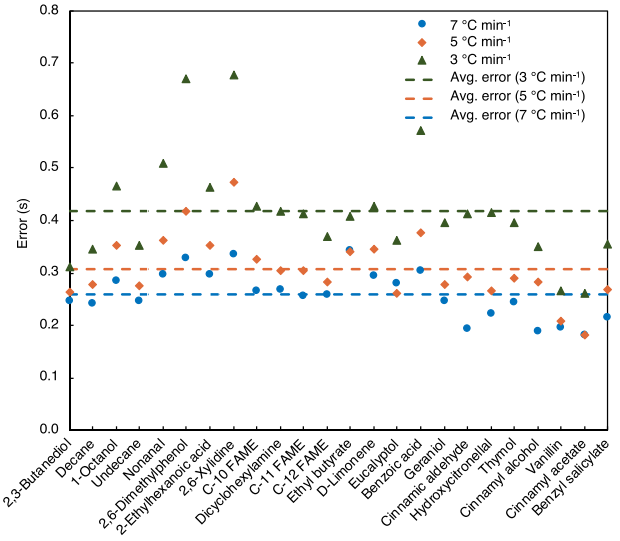

Figure 3. Second-dimension retention time (^2t_r) modeling errors for the 24 studied compounds using three different temperature ramps (7, 5, and 3 °C min^{-1}) and a 4 s modulation period P_M.

increased for all studied compounds when slower programming rates were used, suggesting that the errors are most likely linked to the analytes' elution temperatures. For instance, the average error increased from 0.26 to 0.42 s when the ramp rate was decreased from 7 to 3 °C min^{-1} (Table 2 and Figure 3). The GC temperature profile non-idealities could be the origin of this trend. In fact, numerous works have depicted the existence of small differences between the preset and actual temperature profiles in GC.[31,32] Commonly, the elution temperature decreases when the programming rate decreases. Based on the current trend, it is believed that the temperature difference is more prominent at lower temperatures and therefore affects more perceivably lower T_{el}, resulting in higher modeling errors when smaller ramps are used. Furthermore, 2,6-dimethylphenol, 2,6-xylidine, and benzoic acid seem to be the most affected by this temperature difference. Their modeling errors doubled when the temperature ramp was decreased from 7 to 3 °C min^{-1} (Table 2 and Figure 3). In fact, the GC column used in this study, that is, Rxi-17Sil MS, is characterized by a higher selectivity toward aromatic compounds. The errors made on T_{el} will typically lead to the mischaracterization of the GC equilibrium constant, therefore impacting the accuracy of the modeling, especially for the previously mentioned aromatic compounds.

Usually, the optimal heating rate for a 1D-GC separation is defined as 10 divided by the dead time (in minutes).[33] In the present GC × GC setting, if we assume that the total dead time is no other than the dead time of the ^{1}D column (the ^{2}D column dead time is assumed to be so small that it would not cause a substantial change in the total dead time of the GC × GC setting), 7 °C min^{-1} would be the ideal programming rate for the separations. Therefore, the average modeling error (0.42 s) obtained when using a heating rate of 3 °C min^{-1} (Table 2) can be considered as the upper limit for the modeling error associated with the present model. In fact, a further decrease in the heating rate will undoubtedly lead to a decrease in sensitivity and a significant increase in the total runtime.

By combining the separately predicted ^1t_r and ^2t_r, the elution profile of all compounds was accurately reproduced (Figure 4). Additionally, the predicted chromatograms displayed similar space occupation patterns compared to the experimental ones (Figure 4 and Table 3). The experimental and predicted used retention spaces were studied using the convex hull approach defined by Delaunay triangulation algorithms.[34] The area of the used retention space (measured or predicted) corresponds to the area of the produced convex hull calculated by summing the areas of all generated triangles. The total available retention space is defined using the same approach described by Semard *et al.*[35] It is delimited by the ^{1}D column dead time (^1t_m), the ^1t_r of the last eluting compound, and the modulation period, P_m. The percentages of separation space occupation for both samples are displayed in Table 3. They are calculated by dividing the area of the used retention space by that of the total available retention space.

Interpretation of the Modeling Errors and Model Limitations. So far, the modulator impact on the separation was disregarded from the present modeling approach except for the constraint made on the predicted ^2t_r to not exceed the chosen P_m value. Therefore, it can be attested that the modeling errors are no doubt linked to the omission of the modulator in the modeling process. In an attempt to identify the modulator-related parameters that can help make sense of these errors, it was believed, at first, that the holdup time in the modulator (as a result of the cold trapping) might explain the underestimated retention times. Commonly, the time the analytes spend trapped by the cold jets in the modulator is not accounted for in the reconstructed experimental chromatogram and therefore cannot explain the modeling errors witnessed in the present approach. Furthermore, the results displayed in Table 2 corroborate this assumption that a change in the modulation period duration did not seem to extensively impact the modeling errors for most of the studied compounds. Hence, this assumption was readily disregarded.

In a typical GC × GC framework, the ^{2}D separation is regulated by three distinct temperature profiles emanating from the modulator, the secondary oven, and the transfer line. Nevertheless, in this work, the modeling approach does not account for the temperature changes occurring in these three different segments except for the ^{2}D temperature offset that is included in the final elution temperature but rather assumes that the analytes are separated isothermally at their first-dimension T_{el}. Furthermore, an error on the ^{2}D preset offset temperature cannot be firmly excluded especially since Jaramillo and Dorman have proven its existence.[15] Temperature discrepancies can also lead to mischaracterizations of the thermodynamics-related parameters (eq 9) and impact the retention factor calculations (eq 10).

As an attempt to ease the calculation process, temperature variations arising from the "catch and release" process occurring in the modulator due to the cold and hot jets are not considered in the calculations as they are exceedingly difficult to assess in a straightforwardly manner. Furthermore, when the analytes travel through the modulator to the transfer line passing by the secondary oven, temperature equilibration does not occur instantaneously but fairly takes some time to reach the preset values. This equilibration time is strongly believed to be one of the greatest contributors to the modeling errors.

The carrier gas velocity is also affected by the temperature variations as it increases with increasing temperature. The cold

https://doi.org/10.1021/acs.analchem.2c03107
Anal. Chem. 2022, 94, 17081−17089

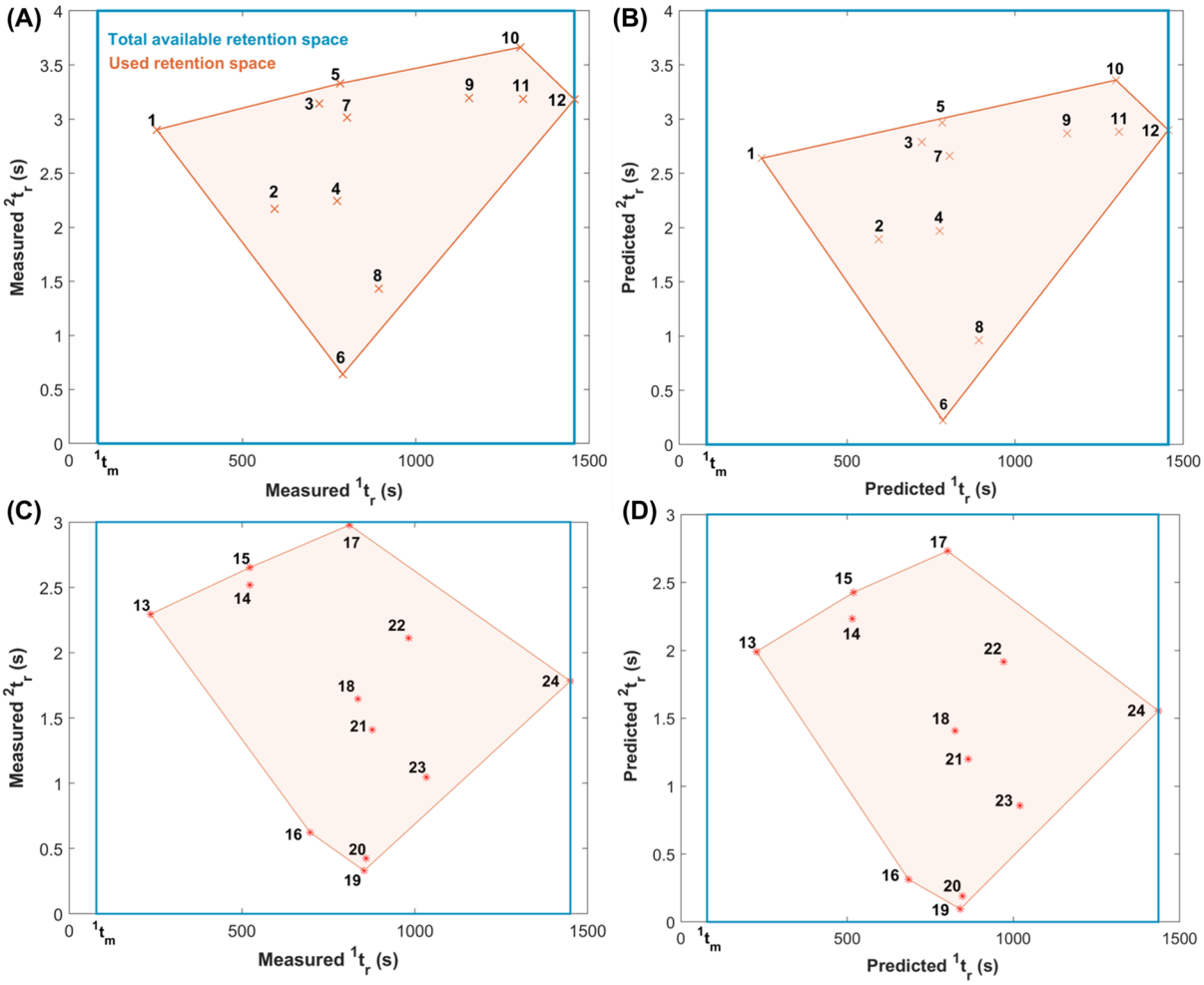

Figure 4. Comparison between the experimental (A,C) and predicted (B,D) chromatographic retention space occupation of the Grob Test Mix (1−12) and Fragrance Materials Test Mix (13−24) compounds. (A) was generated using a 5 °C min^{-1} ramp rate and a 4 s modulation period. The same conditions were used to model (B). (C) was generated using a 7 °C min^{-1} ramp rate and a 3 s modulation period. The same conditions were used to model (D). (1) 2,3-Butanediol, (2) decane, (3) 1-octanol, (4) undecane, (5) nonanal, (6) 2,6-dimethylphenol, (7) 2-ethylhexanoic acid, (8) 2,6-xylidine, (9) C-10 FAME, (10) dicyclohexylamine, (11) C-11 FAME, (12) C-12 FAME, (13) ethyl butyrate, (14) D-limonene, (15) eucalyptol, (16) benzoic acid, (17) geraniol, (18) cinnamic aldehyde, (19) hydroxycitronellal, (20) thymol, (21) cinnamyl alcohol, (22) vanillin, (23) cinnamyl acetate, and (24) benzyl salicylate.

Table 3. Percentages of the Separation Space Used by the Grob Test Mix and the Fragrance Materials Test Mix Compounds When Using Three Different Temperature Ramps[a]

	% separation space occupation					
	7 °C min^{-1}		5 °C min^{-1}		3 °C min^{-1}	
sample	exp.	pred.	exp.	pred.	exp.	pred.
Grob mix	24.53	23.72	32.21	33.32	45.44	44.21
Fragrance mix	44.93	44.60	46.35	47.28	47.33	48.51

[a]All measurements were performed using a modulation period equal to 4 s.

trapping endured by the analytes when traveling through the modulator most likely affects the temperatures they experience. In fact, the actual temperatures are likely to be smaller than their preset counterparts resulting in increased retention and more precisely higher retention times. Consequently, errors in calculating the carrier gas velocity will arguably affect the modeling accuracy causing an underestimation of the ^2t_r.

It is important to highlight that theoretical models, in general, and GC × GC retention time prediction approaches, in particular, are not necessarily bounded to mimic to the last detail the experimental conditions nor to provide retention times that strictly overlap with the measured values but rather to give a range of possible values that would enable the user to have a clearer idea of the spatial distribution of the analytes of interest and therefore to choose the appropriate settings for the separation.

CONCLUSIONS

In this modeling approach, we have successfully demonstrated that an accurate description of the analytes' two-dimensional retention space occupation could be achieved by breaking down the GC × GC system into separate individual 1D-GC subsystems. Particular attention was devoted to modeling the second-dimension retention times of 24 analytes using a total of 9 experimental conditions. The top-down modeling approach discussed in this contribution provided an average ^2t_r modeling error of 0.26 (±0.01 s). However, we demonstrated that a decrease in the heating rate leads to an

https://doi.org/10.1021/acs.analchem.2c03107
Anal. Chem. 2022, 94, 17081−17089

increase in the ^2t_r modeling errors to a maximum average error of 0.42 (±0.02 s). This increase was attributed to temperature differences between the preset and actual GC temperature program with a more prominent discrepancy at lower temperatures. So far, even though the modulator role in the GC × GC separation was omitted in this work, the top-down modeling approach showed quite promising results in terms of the accurate description of the separation space occupation. It offers a new take on retention time modeling in GC × GC, in that it treats the chromatographic separation as two individual one-dimensional separations, in opposition to earlier investigations that mainly focused on modeling the integrity of the two-dimensional separation. Moreover, since the modulator is solely considered as a second consecutive injection device, the top-down approach significantly eases the calculation process and helps circumvent, to a certain extent, the hurdles brought by the acknowledgment of the modulator portion during the modeling process. It is also worth mentioning that this approach can be viewed as system-independent and hence could be worth extending to other multidimensional systems, such as multidimensional liquid chromatography, to say the least. Nevertheless, for future work, we intend to shed light on the temperature variations entailed by the cold and hot jets in the modulator by estimating to a certain extent the equilibration time needed for the temperature to reach the preset value. Additionally, the model's performance will be further investigated for a larger number of compounds spanning a wider range of chemical families. Furthermore, the model's accuracy will also be evaluated using additional GC × GC operating conditions, that is, different column phase combinations and column lengths and different flow rates and temperature programs.

■ ASSOCIATED CONTENT

Supporting Information

The Supporting Information is available free of charge at https://pubs.acs.org/doi/10.1021/acs.analchem.2c03107.

Measured and predicted second-dimension retention times (^2t_r) for the 24 studied compounds using 3 different temperature ramps (7, 5, and 3 °C min^{-1}) and a 4 s modulation period (PDF)

■ AUTHOR INFORMATION

Corresponding Author

Meriem Gaida − *Molecular Systems, Organic and Biological Analytical Chemistry Group, University of Liège, 4000 Liège, Belgium;* orcid.org/0000-0003-4932-472X; Email: Meriem.gaida@uliege.be

Authors

Flavio A. Franchina − *Department of Chemistry, Pharmaceutical, and Agricultural Sciences, University of Ferrara, 44121 Ferrara, Italy*

Pierre-Hugues Stefanuto − *Molecular Systems, Organic and Biological Analytical Chemistry Group, University of Liège, 4000 Liège, Belgium;* orcid.org/0000-0002-1224-8869

Jean-François Focant − *Molecular Systems, Organic and Biological Analytical Chemistry Group, University of Liège, 4000 Liège, Belgium;* orcid.org/0000-0001-8075-2920

Complete contact information is available at: https://pubs.acs.org/10.1021/acs.analchem.2c03107

Funding

This research was funded by the FWO/FNRS Belgium EOS Grant 30897864 "Chemical Information Mining in a Complex World".

Notes

The authors declare no competing financial interest.

■ ACKNOWLEDGMENTS

The authors would like to thank LECO Corporation for its instrumental support.

■ REFERENCES

(1) Liu, Z.; Phillips, J. B. *J. Chromatogr. Sci.* **1991**, *29*, 227−231.
(2) Di Giovanni, N.; Meuwis, M. A.; Louis, E.; Focant, J. F. *J. Proteome Res.* **2020**, *19*, 1013−1028.
(3) Stefanuto, P. H.; Perrault, K. A.; Stadler, S.; Pesesse, R.; LeBlanc, H. N.; Forbes, S. L.; Focant, J. F. *Anal. Bioanal. Chem.* **2015**, *407*, 4767−4778.
(4) Zou, Y.; Gaida, M.; Franchina, F. A.; Stefanuto, P. H.; Focant, J. *Molecules* **2022**, *27*, 1806.
(5) Prebihalo, S. E.; Berrier, K. L.; Freye, C. E.; Bahaghighat, H. D.; Moore, N. R.; Pinkerton, D. K.; Synovec, R. E. *Anal. Chem.* **2018**, *90*, 505−532.
(6) Harynuk, J.; Górecki, T. *Am. Lab.* **2007**, *39*, 36−39.
(7) Dorman, F. L.; Schettler, P. D.; English, C. M.; Patwardhan, D. V. *Anal. Chem.* **2002**, *74*, 2133−2138.
(8) Lu, X.; Kong, H.; Li, H.; Ma, C.; Tian, J.; Xu, G. *J. Chromatogr. A* **2005**, *1086*, 175−184.
(9) Dorman, F. L.; Schettler, P. D.; Vogt, L. A.; Cochran, J. W. *J. Chromatogr. A* **2008**, *1186*, 196−201.
(10) McGinitie, T. M.; Harynuk, J. J. *J. Chromatogr. A* **2012**, *1255*, 184−189.
(11) Zhu, S.; He, S.; Worton, D. R.; Goldstein, A. H. *J. Chromatogr. A* **2012**, *1233*, 147−151.
(12) Barcaru, A.; Anroedh-Sampat, A.; Janssen, H. G.; Vivó-Truyols, G. *J. Chromatogr. A* **2014**, *1368*, 190−198.
(13) Silva, A. C. A.; Ebrahimi-Najafadabi, H.; McGinitie, T. M.; Casilli, A.; Pereira, H. M. G.; Aquino Neto, F. R.; Harynuk, J. J. *Anal. Bioanal. Chem.* **2015**, *407*, 4091−4099.
(14) Burel, A.; Vaccaro, M.; Cartigny, Y.; Tisse, S.; Coquerel, G.; Cardinael, P. *J. Chromatogr. A* **2017**, *1485*, 101−119.
(15) Jaramillo, R.; Dorman, F. L. *J. Chromatogr. A* **2018**, *1581−1582*, 116−124.
(16) Jaramillo, R.; Dorman, F. L. *J. Chromatogr. A* **2020**, *1612*, 460696.
(17) Stevenson, K. A. J. M.; Blumberg, L. M.; Harynuk, J. J. *Anal. Chim. Acta* **2019**, *1086*, 133−141.
(18) McGinitie, T. M.; Ebrahimi-Najafabadi, H.; Harynuk, J. J. *J. Chromatogr. A* **2014**, *1325*, 204−212.
(19) Blumberg, L. M. *J. Chromatogr. A* **2017**, *1491*, 159−170.
(20) Thewalim, Y.; Aldaeus, F.; Colmsjö, A. *Anal. Bioanal. Chem.* **2009**, *393*, 327−334.
(21) González, F. R. *J. Chromatogr. A* **2004**, *1037*, 233−253.
(22) Snijders, H.; Janssen, H. G.; Cramers, C. *J. Chromatogr. A* **1995**, *718*, 339−355.
(23) Clarke, E. C. W.; Glew, D. N. *Trans. Faraday Soc.* **1966**, *62*, 539.
(24) Beens, J.; Tijssen, R.; Blomberg, J. *J. Chromatogr. A* **1998**, *822*, 233−251.
(25) Pesesse, R.; Stefanuto, P. H.; Schleich, F.; Louis, R.; Focant, J. F. *J. Chromatogr. B: Anal. Technol. Biomed. Life Sci.* **2019**, *1114−1115*, 146−153.
(26) Schleich, F. N.; Zanella, D.; Stefanuto, P. H.; Bessonov, K.; Smolinska, A.; Dallinga, J. W.; Henket, M.; Paulus, V.; Guissard, F.; Graff, S.; Moermans, C.; Wouters, E. F. M.; Van Steen, K.; van Schooten, F. J.; Focant, J. F.; Louis, R. *Am. J. Respir. Crit. Care Med.* **2019**, *200*, 444−453.

(27) Gaida, M.; Franchina, F. A.; Stefanuto, P. H.; Focant, J. F. *J. Chromatogr. A* **2021**, *1651*, 462300.
(28) Blumberg, L. M.*Temperature-Programmed Gas Chromatography*; 1st ed.; Wiley-VCH: Weinheim, 2010.
(29) Nahir, T. M.; Morales, K. M. *Anal. Chem.* **2000**, *72*, 4667−4670.
(30) Weggler, B. A.; Dubois, L. M.; Gawlitta, N.; Gröger, T.; Moncur, J.; Mondello, L.; Reichenbach, S.; Tranchida, P.; Zhao, Z.; Zimmermann, R.; Zoccali, M.; Focant, J. F. *J. Chromatogr. A* **2021**, *1635*, 461721.
(31) Vezzani, S.; Moretti, P.; Castello, G. *J. Chromatogr. A* **1997**, *767*, 115−125.
(32) Vezzani, S.; Moretti, P.; Mazzi, M.; Castello, G. *J. Chromatogr. A* **2004**, *1055*, 151−158.
(33) de Zeeuw, J. *Sep. Sci.* **2014**, *6*, 8−13.
(34) Lee, D. T.; Lin, A. K. *Discrete Comput. Geom.* **1986**, *1*, 201−217.
(35) Semard, G.; Peulon-Agasse, V.; Bruchet, A.; Bouillon, J. P.; Cardinaël, P. *J. Chromatogr. A* **2010**, *1217*, 5449−5454.

https://doi.org/10.1021/acs.analchem.2c03107
Anal. Chem. 2022, 94, 17081−17089